Trans Indian Inst Met (2016) 69(7):1359–1368
DOI 10.1007/s12666-015-0693-7

TECHNICAL PAPER

Sintering Behavior of Nanocrystalline Al6063 Powders Prepared by High-Energy Mechanical Milling

H. Asgharzadeh[1]

Received: 10 June 2015 / Accepted: 20 August 2015 / Published online: 8 January 2016

Abstract Nanocrystalline Al6063 powders were synthesized by high-energy mechanical milling of gas-atomized powders for 22.5 h. The powders were uniaxially compacted at various compaction pressures ranging 200–1325 MPa and then were sintered at temperatures between 550 and 650 °C for 1 h. The densification and microstructural evolutions during both solid phase sintering and supersolidus liquid phase sintering are studied. Ultrafine-grained (UFG) Al alloy compacts show superior sinterability compared with coarse-grained (CG) compacts due to the higher defect density and larger specific surface area of the mechanically-milled powders. The densification parameter and hardness of both CG and UFG Al6063 compacts enhances as the compaction pressure increases. Nevertheless, applying high compaction pressures has an adverse effect on the sintered density and results in the swelling of compacts. The results point out an optimum sintering temperature at ~600 °C for achieving the highest sintered density and hardness with minimal grain coarsening and slumping.

Keywords Al6063 · Ultrafine-grained material · Sintering · Densification · Microstructure

1 Introduction

Al alloys have been widely used in aerospace and automotive industries due to their lightweight, high specific mechanical strength, high thermal and electrical conductivities, machinability, and good corrosion resistance [1, 2]. Powder metallurgy (PM) is a near net-shape process that offers an inexpensive route for manufacturing Al parts and serves as a viable processing alternative to casting and forming operations. Nonetheless, fabrication of PM Al components is challenging owing to the presence of a 50–150 Å thick, firm and thermodynamically stable oxide layer covering the powder particles preventing both compressibility and sinterability [3]. Many attempts have been made to enhance densification of Al alloys. It has been reported that densification can be improved by controlling the sintering atmosphere and heating mode [4–6] as well as the addition of reducing agents like Mg [7, 8]. Nonetheless, the successful removal of the oxide layer and sintering of Al parts effectively occurs only in the presence of a liquid phase during sintering [9]. Liquid phase sintering (LPS) usually takes place by heating a mixture of pure or prealloyed Al powder with other elemental powders in order to form a liquid phase between the particles. Such a liquid can penetrate the oxide film through the discontinuities created during compaction, thus facilitating material transport and necks formation between particles [5]. Improvement in the sinterability and mechanical strength through LPS with trace addition of Pb, Sn, Se, Bi and Sb to Al alloys has been stated [10–12]. It has been shown that both 6xxx and 7xxx series Al powder mixture compacts exhibit higher sinterability in comparison to 2xxx series Al alloy compacts [5]. Rapid densification can also be achieved by supersolidus liquid phase sintering (SLPS) in which a prealloyed Al powder compact is heated to a temperature between the solidus and liquidus to form a liquid phase within the particles. Once the liquid spreads to the particle surface, several processes such as rearrangement, solution-precipitation and grain shape accommodation, contribute to the densification [13]. Near full-dense

✉ H. Asgharzadeh
asgharzadeh@tabrizu.ac.ir

[1] Department of Materials Engineering, University of Tabriz, Tabriz 51666-16471, Iran

6xxx series Al alloy compacts have been successfully fabricated via SLPS of prealloyed powder compacts with and without the addition of sintering aids [14–16].

During the last decade, enhancement of the mechanical behavior of Al alloys via grain size refinement has been the subject of intensive research. High-energy mechanical milling is a PM process that is capable of producing nanocrystalline powders through repeated fracture and cold welding of powder particles. Mechanically-milled (MM) Al powder particles are very hard due to their nanocrystalline microstructure and the presence of in situ formed submicroscopic dispersoids [17]. The combination of high hardness and surface oxide/hydroxide layers gives rise to problems in the consolidation step. Several approaches have been employed to consolidate MM Al powders, such as hot pressing [18], hot rolling [19], hot extrusion [20], hot forging [21] and spark plasma sintering [22]. The base of all these methods is to apply high temperature to soften the material and high pressure for densification.

The consolidation of nanocrystalline powders by cold compaction and sintering could be of interest for the production of large batches of small parts [23]. In contrast, sintering alone is infrequently used to consolidate nanocrystalline Al powders, especially Al alloy powders. Cintas et al. [24] have prepared high-density ($\sim$97 % of theoretical density) commercial purity Al parts by cold pressing of MM powders at 850 MPa and vacuum sintering at 650 °C for 1 h. Abdoli et al. [25] have shown that the sinterability of nanocrystalline pure Al compacts improves by degassing treatment at 400 °C and near full dense compacts can be achieved by high-pressure compaction (1.5 GPa) and sintering of degassed powders at 650 °C. Khan et al. [26] have produced commercial-purity Al specimens with relative densities of $\sim$0.97–0.99 and different grain sizes by mechanical milling to different durations followed by degassing, compaction (cold and warm), sintering and annealing. The beneficial effect of LPS on densification of nanocrystalline Al powder particles have been recently investigated by Fuentes et al. [27]. They have reported that blending of the MM Al powder with 0.6 wt% Si as the sintering aid followed by the press and sinter processing, improves both the tensile strength and ductility. The results of previous investigations [24–28] reveal that grain growth is likely to occur during sintering of nanocrystalline powders so that ultrafine-grained (UFG) compacts with grain sizes in the range of 550–850 nm are achieved according to the processing conditions. In the present work, prealloyed Al6063 powder particles were mechanically milled and then consolidated by cold pressing and sintering to produce PM Al alloy parts. The effects of compaction pressure and sintering temperature on the densification and microstructure of UFG Al6063 powder compacts during solid phase sintering and LPS were explored.

2 Experimental Methods

The prealloyed Al6063 powder with the chemical composition of Al–0.92Mg–0.4Si–0.33Fe (in wt%) was prepared by the nitrogen atomization route. The gas-atomized (GA) powder was mixed with 2 wt% Stearic acid (Merck, Germany) as a process control agent (PCA) in a low-energy ball mill for 1 h. Then, high-energy mechanical milling was performed in a planetary ball mill using high-chromium steel vials (125 cm^3 volume) and balls (11 and 19 mm diameter). The ball-to-powder weight ratio of 10:1 and the rotational speed of 350 rpm were employed. Mechanical milling was carried out under Ar atmosphere for 22.5 h.

MM Al6063 powders were degassed in a tube furnace at 400 °C for 1 h. The powders were uniaxially compacted in a rigid steel die to produce 10 mm diameter cylindrical specimens. Compaction was carried out at various pressures between 200 and 1325 MPa. Sintering was performed in a tube furnace in the range of 550–650 °C under Ar atmosphere with the purity of 99.99 %. The compacts were heated at a heating rate of 10 °C min^{-1} to the sintering temperature and were held for 1 h.

Morphology of the powder was studied by field emission scanning electron microscope (FESEM, Tescan, Czech Republic). The tap density of the powder was measured according to the standard ASTM B527. X-ray diffraction (XRD) analysis was performed using a Philips X'pert MPD Diffractometer with Cu K_α radiation source working at 40 kV and 40 mA. Thermal analysis of the powder was conducted by means of Differential scanning calorimetry (DSC, DSC 200 F3 Maia, Netzsch-Gerätebau GmbH., Germany) over the temperature 25–700 °C, at a heating rate of 10 °C min^{-1}. The green density was determined by volumetric method via weight and dimensional measurements. The density of sintered specimens were measured by the Archimedes method. The densification parameter was calculated using the following equation:

$$\text{Densification parameter} = \frac{\text{Sintered density} - \text{Green density}}{\text{Theoretical density} - \text{Green density}}, \quad (1)$$

The powders and sintered compacts were subjected to the metallographic preparation and then etched in Keller's solution (2.5 % HNO_3, 1.5 % HCl, 1 % HF, 95 % H_2O). The microstructure was examined using an optical microscope (OM, Olympus, Japan). Hardness measurements of the samples were performed using Vickers microhardness tester

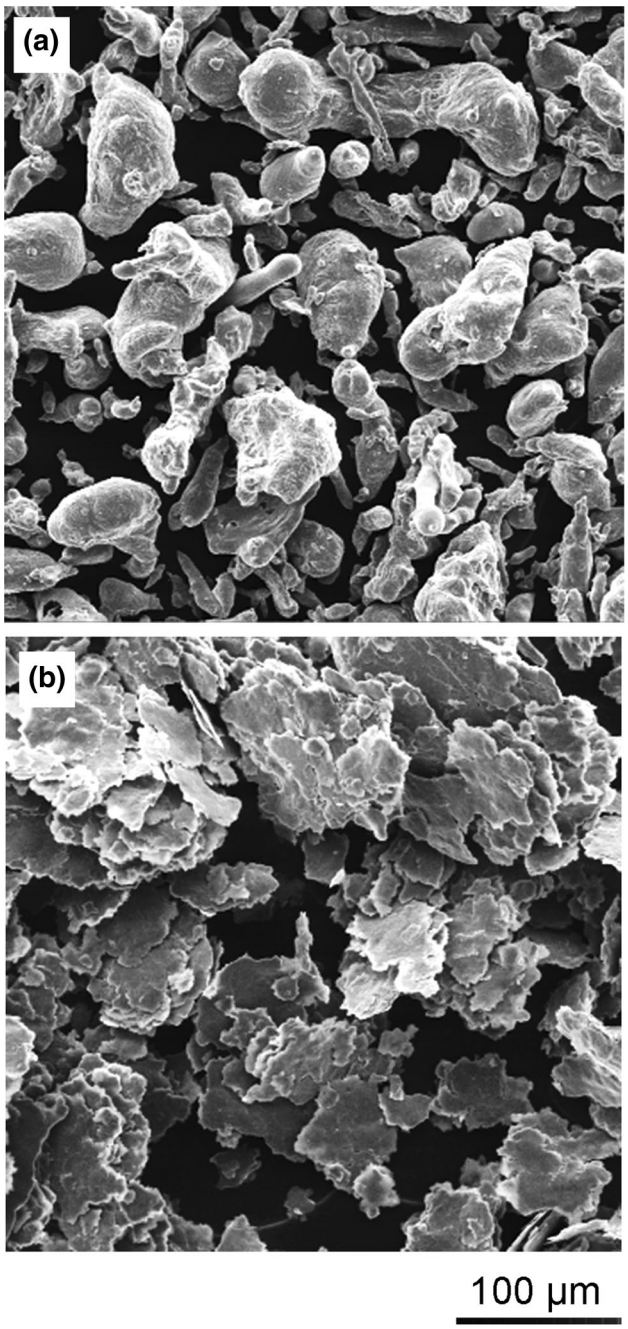

Fig. 1 FESEM images of Al6063 powder particles: **a** GA and **b** MM

(Zwick Roell, ZHv 10, Germany) under the applied load of 4.9 N.

3 Results

3.1 Powder Characteristics

The morphology and microstructure of Al6063 powder after gas atomization and mechanical milling for 22.5 h are

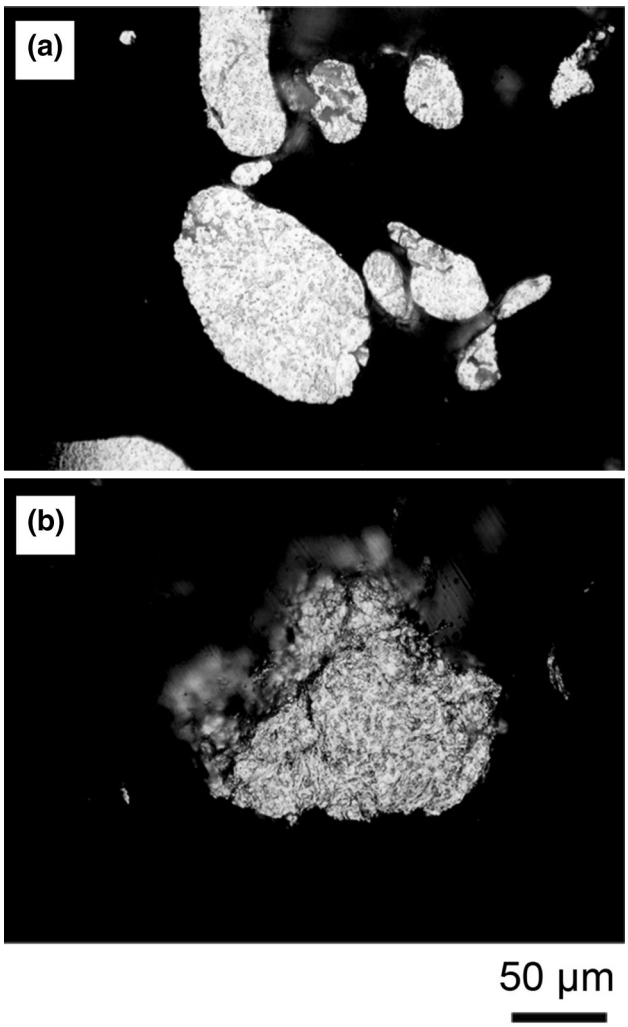

Fig. 2 OM images of Al6063 powder particles: **a** GA and **b** MM

shown in Figs. 1 and 2, respectively. The GA powder has a relatively equiaxed and quasi-spherical morphology with a fine cellular and dendritic microstructure (Figs. 1a, 2a), which is typical of the GA powders. The MM powder shows a stack of flattened particles (Fig. 1b) resulting from the continuous impacts of high-energy balls during mechanical milling. Continuous deformation, welding and fragmentation of powder particles after 22.5 h mechanical milling results in the formation of particles with OM invisible interfacial boundaries within them, as shown in Fig. 2b. The morphological and microstructural evolutions of Al6063 powder particles upon high-energy mechanical milling for various durations have been reported in details elsewhere [29]. It is well established that the density of the powder particles decreases with increasing milling duration at the initial stages of mechanical milling, then increases at longer milling durations and finally reaches a steady value after prolonged milling duration [30]. The tap densities of GA and MM powders were measured as 1.51 and

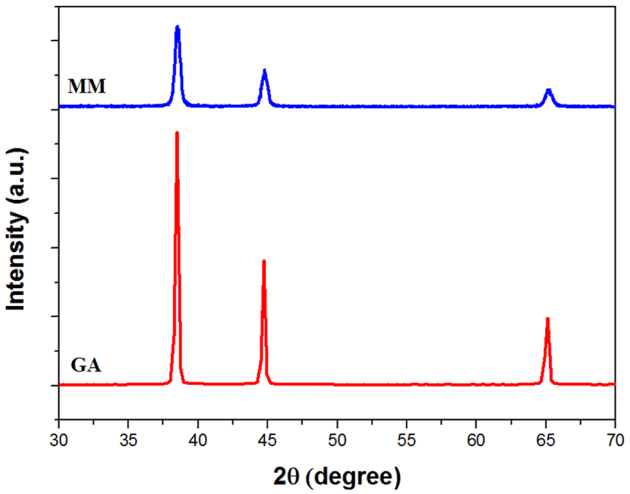

Fig. 3 XRD patterns of Al6063 powders

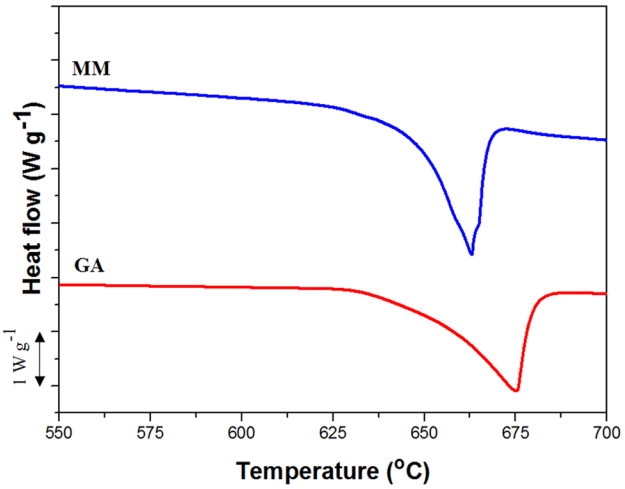

Fig. 4 DSC curves of Al6063 powders

1.43 g cm^{-3}, respectively, indicating close packing characteristics of powder particles, which can be ascribed to the quasi-balance between cold welding and fracture mechanisms during mechanical milling.

Figure 3 demonstrates the XRD patterns of Al6063 powders. The diffraction patterns of both GA and MM powders show the typical reflections for aluminum. It is to be noted that the impurity contamination take place upon high-energy mechanical milling due to the impact of the grinding balls on the vials. The results of atomic analysis of milled Al–Al_2O_3 powders shows that the powders tend to absorb iron at an initial stage of milling and their susceptibility gradually decreases until steady-state condition is prevailed [31]. The presence of iron in Al6063 powders after attrition milling for 20 h is detected as well [29]. Thus, the lack of impurities/second phases in the XRD patterns of the milled powder can be attributed to their low content. The XRD peak line broadening and attenuation are noticed in the MM powder that can be attributed to the grain size refinement and accumulation of the lattice strain. The crystallite size (d) and the microstrain (η) of MM powder were calculated using the Williamson-Hall equation [32]:

$$B\cos\theta = \frac{k\lambda}{D} + 2\eta\sin\theta, \quad (2)$$

where λ is the wavelength of the X-ray ($\lambda CuK_{\alpha 1} = 0.15406$ nm), B is the peak width at half the maximum intensity, θ is the Bragg angle and k is a constant equal to 0.9. The crystallite size and the lattice strain of MM Al6063 powder were determined approximately 38 nm and 0.34, respectively, revealing a significant grain size refinement of GA powder and an accumulation of large strain upon mechanical milling. The microstructural refinement during high-energy mechanical milling is ascribed to the localization of plastic deformation in the form of shear bands, the formation of subgrains/cells, and the conversion of subgrains/cells into grains through subgrain boundary sliding and grain rotation [33].

The applicability of the prealloyed powder for LPS can be assessed based on the development of liquid phase by increasing the temperature via DSC analysis (Fig. 4). DSC curves of Al6063 show a single endothermic event at 675 and 663 °C for GA and MM powders, respectively, related to the melting of alloys. A similar shift in the position of DSC peak after mechanical milling has been previously reported by Abdoli et al. [34]. It is well established that the melting temperature of nanostructured solids decreases with decreasing their crystal size [35]. Thus, a shift in the melting temperature of powders towards lower temperature

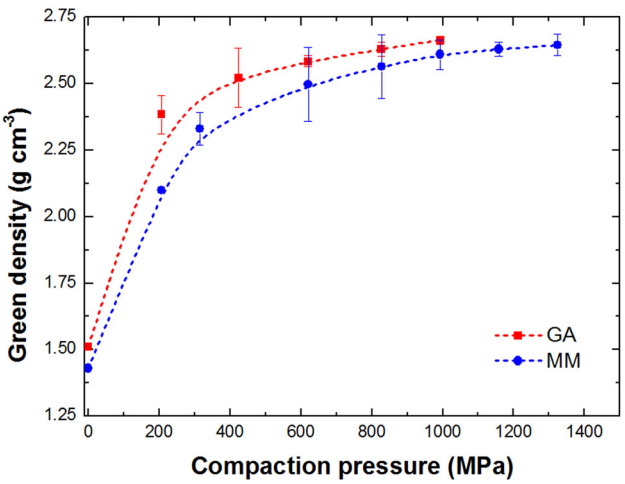

Fig. 5 The variation of green density with applied compaction pressure

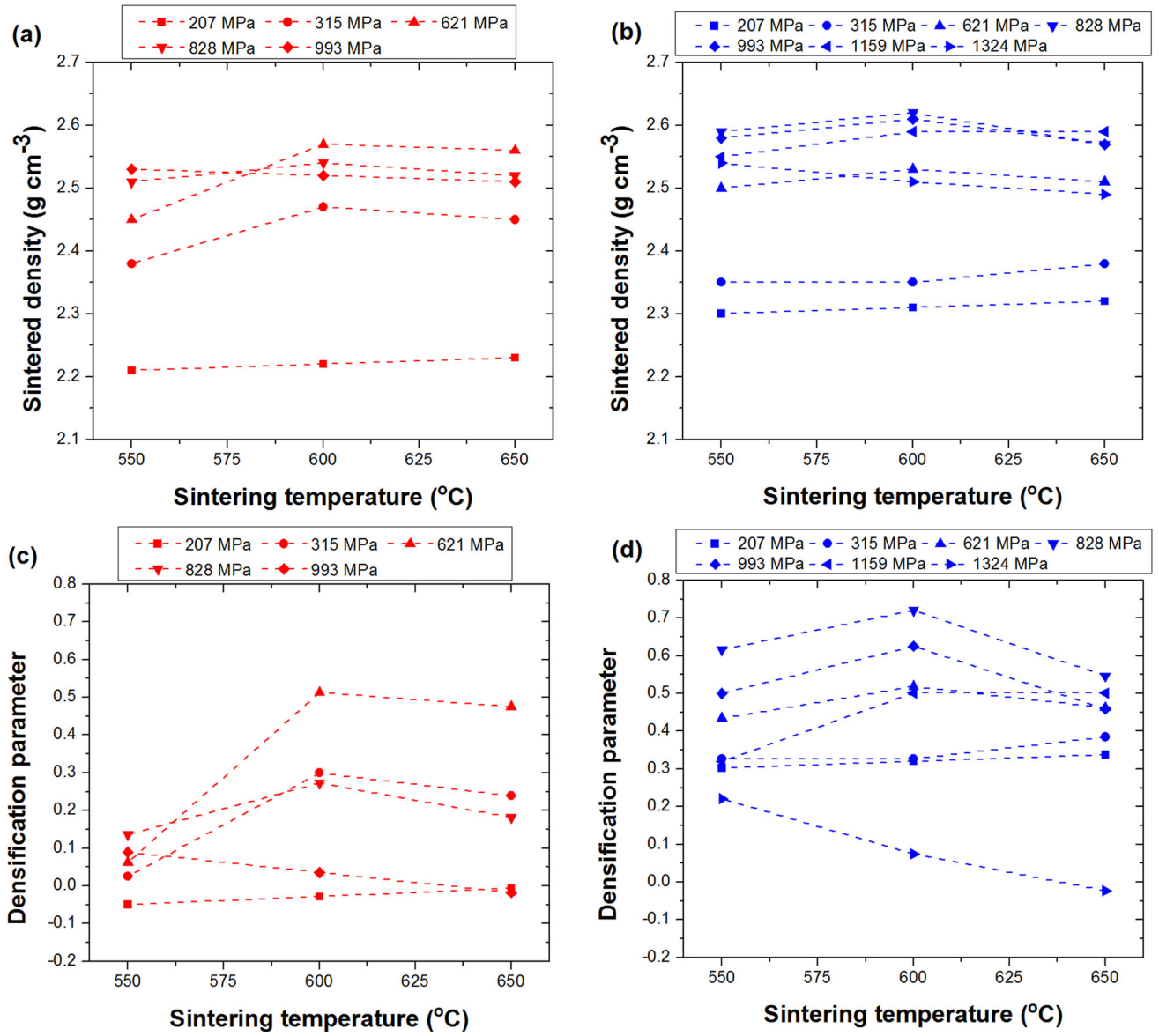

Fig. 6 The sintered density and the densification parameter of CG (**a**, **c**) and UFG (**b**, **d**) Al6063 compacts as a function of the sintering temperature

after mechanical milling can be attributed to the grain size refinement to the nanoscale level.

3.2 Sintering Behavior

Figure 5 illustrates the variation of green density of Al6063 powders as a function of compaction pressure. The density at P = 0 is consistent to the tap density of the powders. As the compaction pressure increases, the density increases. However, the densification rate is significantly reduced at higher pressures (>∼300 MPa) indicating a change in the densification mechanism from particle rearrangement to plastic deformation. Additionally, MM Al alloy powder shows a lower compressibility compared with GA powder.

Figure 6 elucidates the variations in sintered density and densification parameter of coarse-grained (CG) and UFG Al6063 compacts prepared from GA and MM powders, respectively, with the sintering temperature. It can be seen that the sintered density and the densification parameter of the specimens compacted at low pressures (e.g. 207 MPa) improves by increasing the sintering temperature from 550 to 650 °C. Nevertheless, the highest sinterability is attained at 600 °C for the compacts consolidated at moderate compaction pressures, i.e. 315–828 and 621–1159 MPa for CG and UFG compacts, respectively. Finally, increasing the sintering temperature creates an adverse effect on the sintered density and the densification parameter of the specimens prepared under high compaction pressures (e.g.

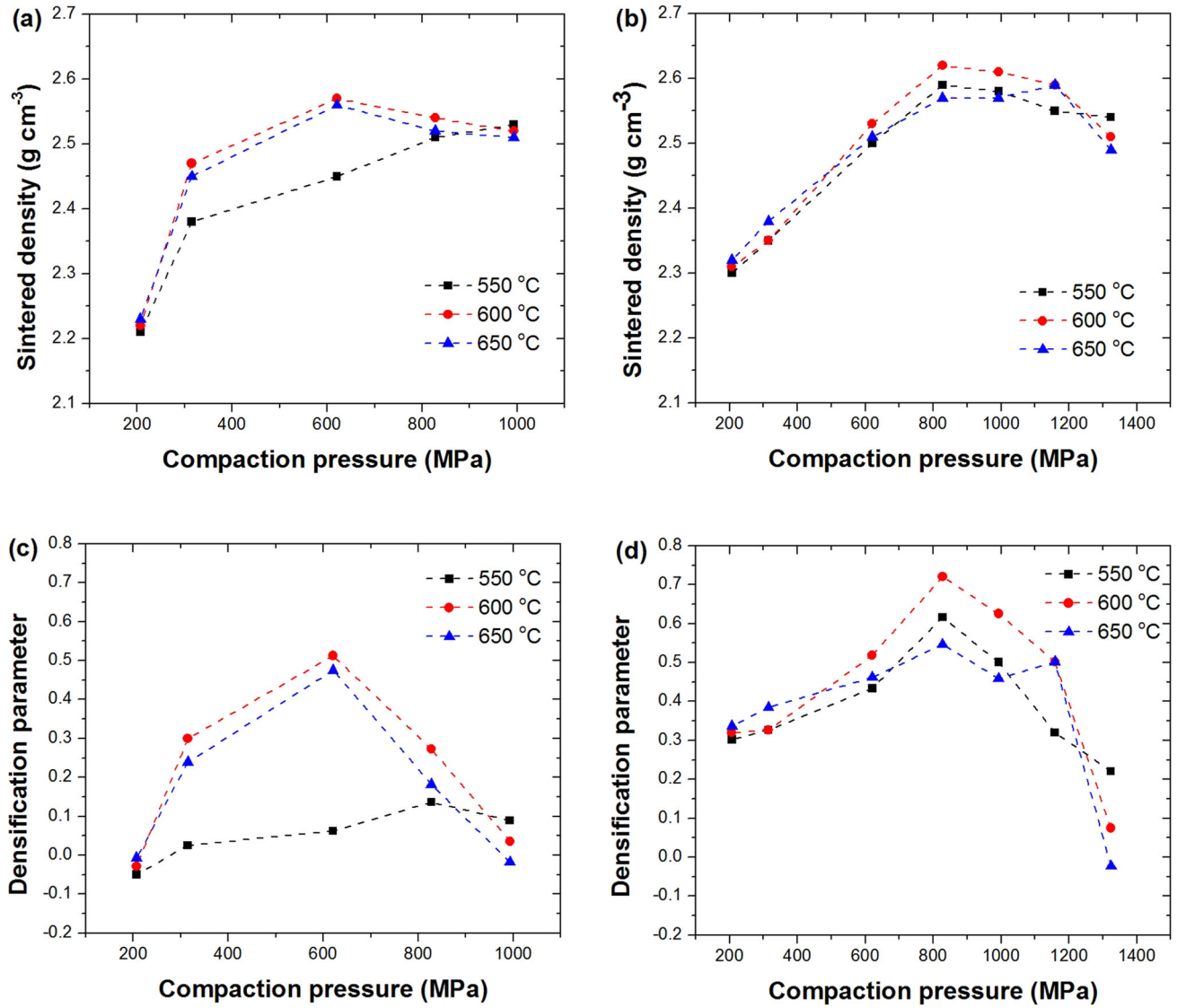

Fig. 7 The changes of sintered density and densification parameter with the compaction pressure for CG (**a**, **c**) and UFG (**b**, **d**) Al alloy compacts sintered at various temperatures

993 and 1324 MPa for CG and UFG compacts, respectively). Thus, the compaction pressure has a significant role in the sintering response of both GA and MM Al6063 powders. For an assessment of this incident, the effects of compaction pressure on the sinterability of Al6063 compacts are shown in Fig. 7. The sintered density and densification parameter of CG compacts sintered at 550 °C improves as the compaction pressure increases. Nonetheless, in the case of compacts sintered at 600 and 650 °C, there is an optimal densification at the compaction pressure of 621 MPa. Similarly, the highest sintered density and densification parameter of UFG compacts are accomplished for the specimens which are compacted at 828 MPa for the full sintering temperature range. It is clear from Fig. 7 that the maximum densification parameter for the UFG compact (~0.72) is larger than that of the CG compact (~0.51). Meanwhile, the peak density of UFG compacts is slightly higher than the peak density of CG parts.

The effects of compaction pressure and sintering temperature on the microstructure of CG Al6063 specimens are depicted in Fig. 8. The microstructure of specimens compacted at 207 MPa indicates equiaxed grains and high porosity. The amount of porosity significantly reduces on increase in the compaction pressure. Furthermore, relatively flattened grains with well-developed interparticle bonds are observed in the specimens compacted at 993 MPa and sintered at 550 and 600 °C (Fig. 8d, e). Increasing the sintering temperature give rise to the reduction of prior particle boundaries (PPBs), development

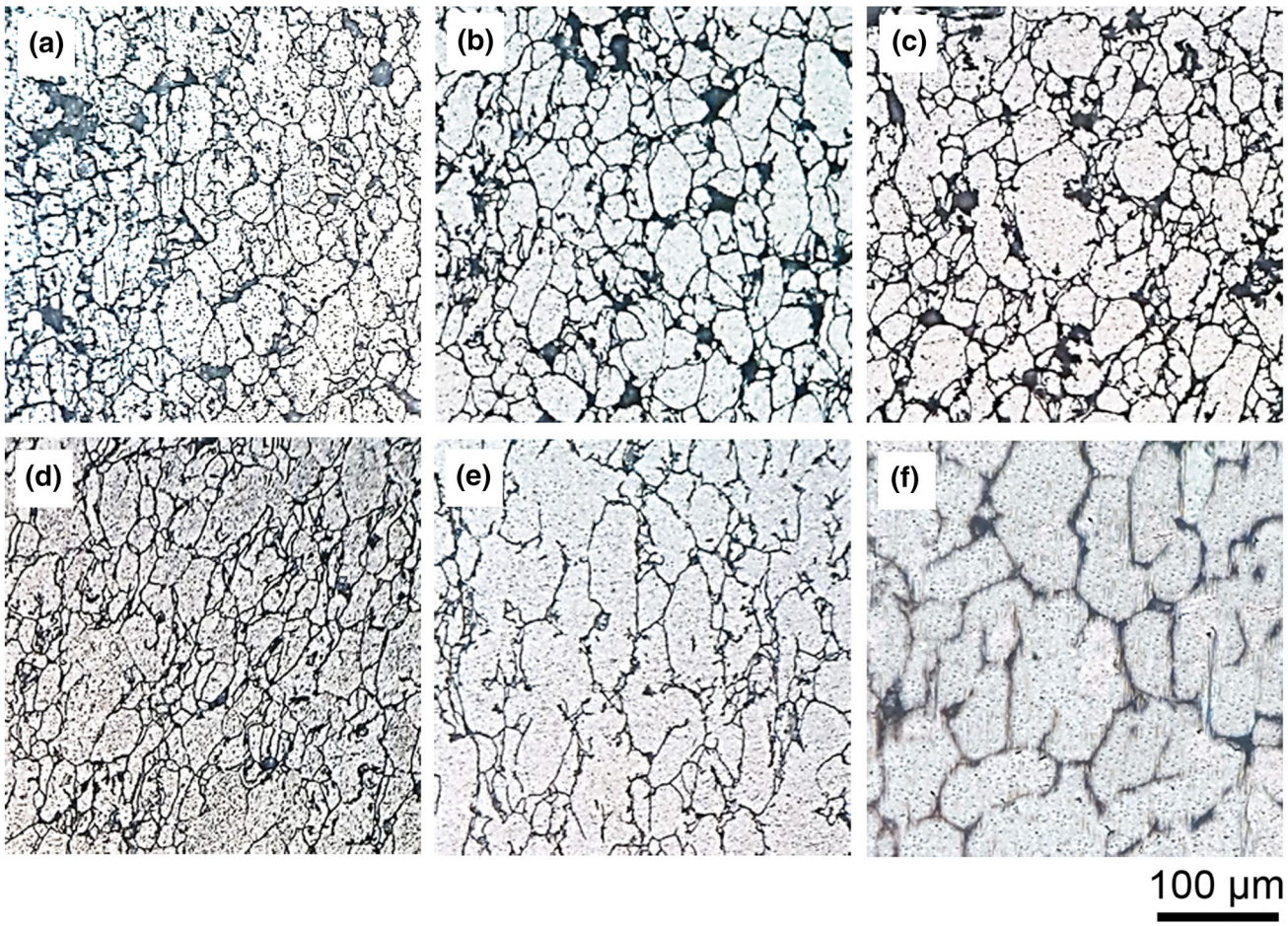

Fig. 8 Optical micrographs of CG Al6063 specimens compacted and sintered at various conditions: **a** 207 MPa/550 °C; **b** 207 MPa/600 °C; **c** 207 MPa/650 °C; **d** 993 MPa/550 °C; **e** 993 MPa/600 °C; **f** 993 MPa/650 °C

of more interparticle bonds and grain coarsening, especially with the application of higher compaction pressures (Fig. 8f).

The representative microstructures of the UFG compacts prepared by pressing and sintering of MM Al6063 powders at various conditions are illustrated in Fig. 9. The microstructure of UFG Al6063 specimens consist of relatively layered, well-bonded and inhomogeneous grains. It has been shown elsewhere that the contrast between the grains is due to their size difference [36]. Whereas finer grains are more susceptible to the etch reagent, coarse grains and ultrafine grains are represented by bright and dark areas, respectively. By comparing Fig. 9 with 8, it can be seen that the interparticle porosity of UFG compacts is less than that of CG specimens prepared at similar conditions. When the compaction pressure increases from 207 to 993 MPa, the amount of porosity decreases and the grains are more flattened. The fraction of CGs raises as the sintering temperature increases, revealing the significant grain coarsening at higher sintering temperatures. Swelling and even cracking of the specimens occurs at the sintering temperature of 650 °C irrespective of the level of compaction pressure. Furthermore, the UFG compacts sintered at 600 °C swells only when high compaction pressures are applied.

Figure 10 shows the hardness of sintered Al6063 specimens prepared at various conditions. In the case of CG specimens compacted at 207 MPa, the hardness value enhances with the increase in the sintering temperature (Fig. 10a). Nevertheless, there is a peak hardness at the sintering temperature of 600 °C for the specimens compacted at higher pressures. The highest hardness value ($\sim$58 Hv) is attained for the specimen compacted at 621 MPa and sintered at 600 °C. The hardness of UFG specimens compacted at 207 MPa raises with the increase in the sintering temperature from 550 to 600 °C, however sintering at 650 °C shows an insignificant effect on the hardness (Fig. 10b). Similar to CG compacts, the specimens compacted at 993 MPa shows a peak hardness at the sintering temperature of 600 °C. A further increase in the

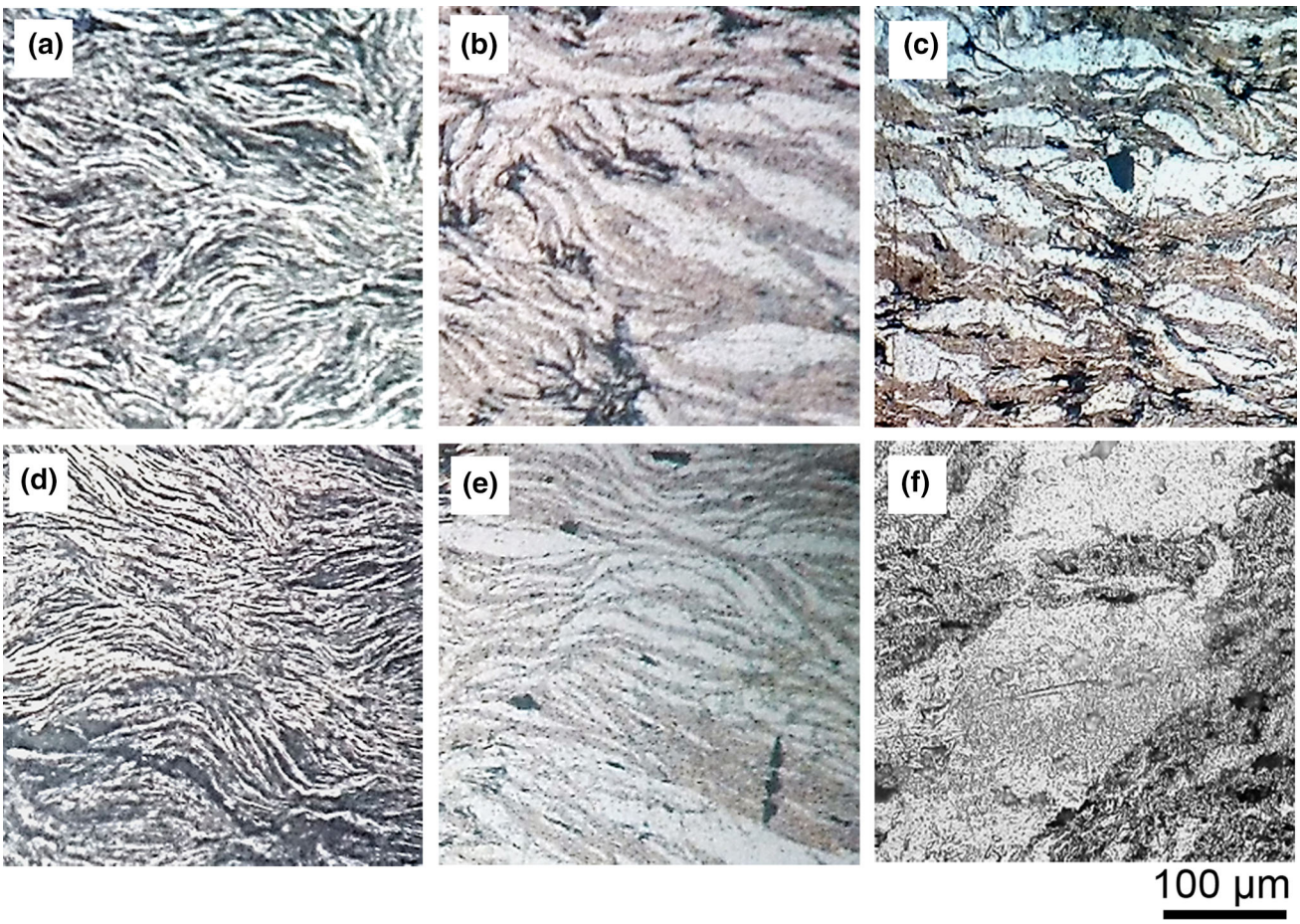

Fig. 9 Optical micrographs showing the microstructure of UFG 6063 Al alloy compacted and sintered at various conditions: **a** 207 MPa/550 °C; **b** 207 MPa/600 °C; **c** 207 MPa/650 °C; **d** 993 MPa/550 °C; **e** 993 MPa/600 °C; **f** 993 MPa/650 °C

compaction pressure results in the reduction of hardness with the increase in sintering temperature. The peak hardness of the UFG compacts (~ 87 Hv) is achieved at the compaction pressure of 993 MPa and the sintering temperature of 600 °C.

4 Discussion

The sintering behavior of prealloyed Al6063 was significantly affected by high-energy mechanical milling prior to consolidation. The results indicated that MM Al alloy powders showed an enhanced sinterability compared to GA powders resulted in a higher sintered density in the UFG compacts (Figs. 6, 7). This might be ascribed to the high defect density (e.g. dislocations and grain boundaries) and large specific surface area of the MM powder particles that could provide an additional driving force and promote the densification during sintering [37]. According to Fig. 10, not only the sinterability, but also the mechanical properties of the compacts were considerably influenced by mechanical milling processing; the hardness of UFG Al6063 specimens was 18–50 % superior than that of CG Al6063 compacts according to the processing condition. The higher mechanical properties of the sintered UFG Al6063 alloy compared with that of the CG material was in agreement with our previous work in which hot powder extrusion was used for consolidation of MM Al6063 powders [38]. The enhanced hardness of UFG Al6063 compacts could be related to the refined microstructure with a high fraction of high-angle boundaries, second phase particles (precipitates and in situ formed particles upon mechanical milling), and a high density of thermal mismatch and geometrically necessary dislocations [39].

It was shown that compaction pressure and sintering temperature had a noteworthy effect on the densification, microstructure and hardness of both CG and UFG Al6063 compacts. There was an optimal compaction pressure that gave rise to the highest sintered density and hardness in Al6063 compacts. According to the results presented in Fig. 7, the most favorable compaction pressure for the GA and MM powders was approximately 621 and 828 MPa,

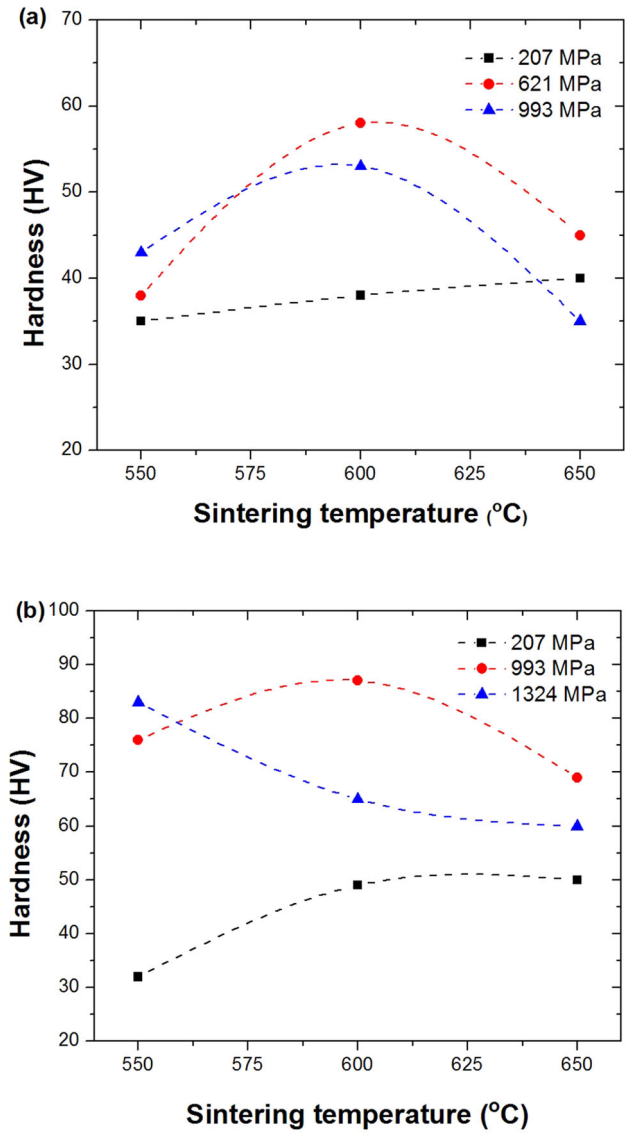

Fig. 10 Hardness of Al6063 compacts as a function of sintering temperature at various compaction pressures: **a** CG compacts and **b** UFG compacts

respectively, which resulted in a green density of ~90 % for both Al alloy powder compacts. The necessity for a higher pressure for compaction of MM powders compared with GA powders was mainly due to the lower compressibility of the milled powders. In fact, high-energy mechanical milling degraded the plastic deformation propensity of the GA powders due to the grain size refinement, accumulation of lattice strain and fine dispersion of particles (e.g. Al_2O_3 and Al_4C_3) [40, 41]. The experimental results revealed that, when an intermediate compaction pressure was employed, the highest sinterability, density and hardness was achieved at the sintering temperature of 600 °C. The reduction in the sintered density when a higher sintering temperature (650 °C) was employed could be related to the lower capillary flow of the liquid during SLPS, as will be explained later.

It was found that applying low compaction pressures could not effectively break down the oxide layers on the Al alloy powders which caused the formation of weak sinter-necks between Al particles during sintering and leaving a high amount of interparticle porosities (Figs. 8, 9). Thus, sintering at higher temperatures, improved the densification and hardness of compacts, as shown in Figs. 6 and 10. It was well established that the formation of a liquid phase along the grain boundaries of a prealloyed powder upon sintering significantly contributed in the densification and the amount of liquid directly influenced the kinetics of densification [42]. According to the DSC curves (Fig. 4), the onset melting temperature for CG and UFG compacts is approximately 648 and 644 °C, respectively. Thus, when sintering was performed at 550 and 600 °C, no liquid phase was formed in the sintered microstructures revealing the prevalence of solid-state sintering mechanism. In contrast, increasing the sintering temperature to 650 °C resulted in the promotion of SLPS mechanism. The creation of a liquid phase along the grain boundaries and inter-particle contacts caused a disintegration of the rigid solid skeleton and provided both capillary force and diffusion medium for densification. Hence, the sintered density increased and the microstructure showed a little amount of porosity (Figs. 8c, 9c). On the other hand, low densification was achieved when compaction pressures beyond the threshold pressure were employed. The degraded sinterability could be attributed to the presence of higher trapped gas in the pores and the lower capillary flow of the liquid during SLPS at higher green densities [42]. In fact, the amount of trapped gas in the pores between the Al powder particles increased as higher compaction pressures were applied. Under this condition, the growth of the pores during sintering took place. In contrast, it is known that high green densities have an adverse effect on the capillary flow of the liquid during SLPS. Therefore, driving force for material transfer and diffusion was diminished; thereby the amount of densification was reduced, as shown in Fig. 7. The results showed a transition from densification to swelling by increasing the sintering temperature for Al6063 alloy specimens compacted at high pressures (Fig. 7). Swelling and even cracking of some specimens compacted at very high-pressure levels during SLPS occurred as well (Fig. 9c).

5 Conclusions

Coarse-grained and UFG Al6063 powder compacts were prepared by uniaxial die compaction and sintering. It was shown that CG and UFG Al6061 powder specimens compacted at ~621 and ~828 MPa, respectively, could be

extremely densified during sintering. The sinterability of specimens compacted at lower pressures, was improved at higher sintering temperatures. In contrast, beyond this threshold, increasing the sintering temperature degraded the densification parameter. Nanocrystalline Al alloy powders showed an enhanced sinterability compared with microcrystalline powders which resulted in the higher density and hardness in the UFG compacts. Thus, near full dense ($\sim$97 % of theoretical density) UFG Al6063 compacts were achieved by compaction at 828 MPa and sintering at 600 °C for 1 h.

Acknowledgments The author thanks the University of Tabriz for all of the support provided. The author wish to thank A. Tarasi and P. Pishva for assistance in performing the tests.

References

1. Daver E M, Ullrich W J, and Patel K B, *Key Eng Mater* **29–31** (1989) 401.
2. Stevenson R W, *P/M Lightweight Metals*, ASM Handbook, ASM, Metals Park, USA (1984) 9th Ed., p 741.
3. Schaffer G B, Sercombe T B, and Lumley R N, *Mater Chem Phys* **67** (2001) 85.
4. Jha A K, Prasad S V, and Upadhyaya G S, Powder Metall Int 20 (1988) 18.
5. Martin J M, and Castro F, *J Mater Process Technol* **143–144** (2003) 814.
6. Padmavathi C, Upadhyaya A, and Agrawal D, *Mater Res Innov* **15** (2011) 294.
7. Lumley R N, Sercombe T B, and Schaffer G B, *Metall Mater Trans A* **30** (1999) 457.
8. Kondoh K, Kimura A, and Watanabe R, *Powder Metall* **44** (2001) 161.
9. Padmavathi C, Upadhyaya A, and Agrawal D, *Mater Chem Phys* **130** (2011) 449.
10. Sercombe T B, and Schaffer G B, *Mater Sci Eng A* **268** (1999) 32.
11. Schaffer G B, and Huo S H, *Powder Metall* **42** (1999) 219.
12. Schaffer G B, Huo S H, Drennan J, and Auchterlonie G J, *Acta Mater* **49** (2001) 2671.
13. German R M, *Int J Powder Metall* **26** (1990) 35.
14. Ziani A, and Pelletier S, *Int J Powder Metall* **35** (1999) 49.
15. Youseffi M, and Showaiter N, *Powder Metall* **49** (2006) 240.
16. Asgharzadeh H, and Simchi A, *Powder Metall* **52** (2009) 28.
17. Rodriguez J A, Gallardo J M, and Herrera E J, *J Mater Sci* **32** (1997) 3535.
18. Shanmugasundaram T, Heilmaier M, Murty B S, and Subramanya Sarma V, *Mater Sci Eng A* **527** (2010) 7821.
19. Choi H J, Shin J H, Min B H, and Bae D H, *Compos A* **41** (2010) 327.
20. Asgharzadeh H, Simchi A, and Kim H S, *Mater Sci Eng A* **528** (2011) 3981.
21. Ahn B, Mitra R, Lavernia E J, and Nutt S R, *J Mater Sci* **45** (2010) 4790.
22. Kumar Rana J, Sivaprahasam D, Seetharama Raju K, and Subramanya Sarma V, *Mater Sci Eng A* **527** (2009) 292.
23. Cintas J, Cuevas F G, Montes J M, and Herrera E J, *Scr Mater* **52** (2005) 341.
24. Cintas J, Montes J M, Cuevas F G, and Herrera E J, *J Mater Sci* **40** (2005) 3911.
25. Abdoli H, Asgharzadeh H, and Salahi E, *J Alloys Compd* **473** (2009) 116.
26. Khan A S, Farrokh B, and Takacs L, *Mater Sci Eng A* **489** (2008) 77.
27. Fuentes J J, Rodriguez J A, and Herrera E J, *J Alloys Compd* **484** (2009) 806.
28. Asgharzadeh H, and McQueen H J, *Mater Sci Technol* **31** (2015) 1016.
29. Asgharzadeh H, Simchi A, and Kim H S, *Mater Sci Eng A* **527** (2010) 4897.
30. Fogagnolo J B, Robert M H, and Torralba J M, *Mater Sci Eng A* **426** (2006) 85.
31. Zebarjad S M, and Sajjadi S A, *Mater Des* **27** (2006) 684.
32. Williamson G K, and Hall W H, *Acta Metall* **1** (1953) 22.
33. Zhang D L, *Prog Mater Sci* **49** (2004) 537.
34. Abdoli H, Ghanbari M, and Baghshahi S, *Mater Sci Eng A* **528** (2011) 6702.
35. Qi W H, *Phys B* **368** (2005) 46.
36. Panigrahi B B, *Mater Sci Eng A* **460–461** (2007) 7.
37. Asgharzadeh H, Simchi A, and Kim H S, *Metall Mater Trans A* **42** (2011) 816.
38. Sakoori Oskooie M, Asgharzadeh H, and Kim H S, *J Alloys Compd* **632** (2015) 540.
39. Asgharzadeh H, Simchi A, and Kim H S, *Mater Charact* **75** (2013) 108.
40. Abdoli H, Farnoush H R, Asgharzadeh H, and Sadrnezhaad S K, *Powder Metall* **54** (2011) 24.
41. Asgharzadeh H, Simchi A, and Kim H S, *Powder Technol* **211** (2011) 215.
42. German R M, *Int J Powder Metall* **26** (1990) 23.